Ferromagnetic resonance shifts from electric fields: Field-enhanced screening charge in ferromagnet/ferroelectric multilayers

V. Gunawan[1,2,*] and R. L. Stamps[1,3]

[1]*School of Physics M013, University of Western Australia, 35 Stirling Highway, Crawley, Western Australia 6009, Australia*

[2]*Jurusan Fisika, FMIPA, Universitas Diponegoro, Jl. Prof. Soedarto, Tembalang, Semarang, Indonesia*

[3]*SUPA–School of Physics and Astronomy, University of Glasgow, Glasgow G12 8QQ, United Kingdom*

(Received 31 May 2011; published 15 March 2012)

We calculate standing spin wave frequencies in a multilayer which unit cell is a trilayer comprised of a ferromagnet, a ferroelectric, and a normal metal. An applied voltage enhances the polarization of the ferroelectric and increases the magnetic moment at one interface through spin polarization and charge transfer. We show that the induced surface magnetism results in shifts of resonance and standing spin wave mode frequencies. A new resonance peak is predicted, associated with a strongly localized surface moment. Estimates are provided using parameters appropriate to the ferroelectric $BaTiO_3$ and four different ferromagnetic metals, including a Heusler alloy (Fe, CrO_2, permalloy, and Co_2MnGe). The calculations use an entire-cell effective-medium approximation that takes into account the polarization profile in the ferroelectric. The metallic ferromagnetic electrode is treated as a real metal, and the depolarization field is included in the determination of polarization in the ferroelectric.

DOI: 10.1103/PhysRevB.85.104411 PACS number(s): 75.85.+t, 75.76.+j, 75.30.Ds, 75.30.Cr

I. INTRODUCTION

Manipulation and control of electron spin is the heart of spin electronics. Extensive theoretical studies have been done on the magnetoelectric (ME) effect in composites comprised of metallic ferromagnets (FM) and ferroelectrics (FE) using *ab initio* band-structure calculations,[1] first-principles calculations,[2,3] and calculations of the screening potential.[4,5] In this type of ME effect, polarization by the ferroelectric generates spin-polarized charges at the ferromagnet/ferroelectric interface that change the magnetization at the ferromagnet interface through spin-dependent screening within the ferromagnet layer. Spin is accumulated within a few lattice sites of the interface, creating an additional magnetization. This effect is referred to as interface ME mediated by carriers. Previous studies of carrier-mediated magnetoelectricity[1–5] focused on the calculation of additional magnetization and ME coupling. Tunneling process by the spin-dependent carriers have also been considered.[6]

In the present work, we show how the induced additional magnetization affects spin waves, and can be measured using ferromagnetic resonance. Since the additional magnetization effectively occurs only at the ferromagnet/ferroelectric interface, the electrodes need to be as thin as possible for measurable effects. As a consequence, the spin-polarized charge at the ferroelectric edge cannot be completely compensated by spin-dependent screening charges. This means that the ferromagnet electrode should be treated as a real metal and depolarization should be accounted for in the calculation of polarization in the ferroelectric component. Since there is a depolarization field that tends to suppress polarization, an external electric field is needed to produce stable polarization. Taking these effects into account, we show that there is a small but measurable shift of the resonance frequency. We find also the appearance of an additional weak resonance as a result of the existence of the additional magnetization.

The paper is organized as follows. The theory for screening charge in the trilayer system is given in Sec. II, where we also discuss the effect of incomplete compensation of the polarization. In Sec. III, the additional magnetization is calculated using a Thomas-Fermi approximation based on the theory by Zhang.[4] The effect of additional magnetization on spin wave frequencies and mode profiles is discussed in Sec. IV. Numerical calculations for the magnetic susceptibility using an entire-cell effective-medium theory are given in Sec. V. Frequency shifts as a function of applied field for four different ferromagnetic metals are given in Sec. V. A summary and conclusions are given in Sec. VI.

II. GEOMETRY AND SCREENING CHARGES

In this section, we describe how film thicknesses affect screening charges. The geometry is sketched in Fig. 1. We consider a cell consisting of a trilayer where the ferroelectric is sandwiched between the metallic ferromagnet and the normal metal. The polarization is assumed to be in-plane, opposite to the $\hat{x}$ axis, while the magnetization of the ferromagnet is also in-plane along the $\hat{z}$ axis. Compared to a ferromagnet/ferroelectric/ferromagnet trilayer, the ferromagnet/ferroelectric/normal metal configuration can result in a stronger magnetoelectric effect through spin transfer between the ferromagnet and the normal metal.[5] Polarization in the ferroelectric gives rise to bound charges at the ferroelectric interface. These bound charges are compensated by screening charges in the normal metal electrode. Shorting the electrodes allows spin polarized charge to accumulate at the ferromagnet/ferroelectric interface with charge depletion at the ferroelectric/normal metal interface. Spin polarization is possible because the ferromagnet electrode is a ferromagnetic transition metal and there is some spin polarization of conduction spins. This means that the screening electrons will possess a net magnetic moment, which results in the appearance of additional magnetization. In the ferromagnet/ferroelectric/ferromagnet configuration, the additional magnetization at one interface is compensated by the same decrease of magnetization at the other side, hence

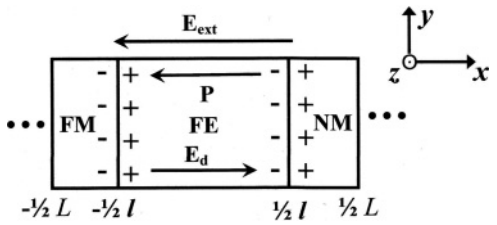

FIG. 1. Geometry of ferromagnet/ferroelectric/normal metal trilayer. The polarization accumulates free charge at ferroelectric interfaces. The charge compensation by electrodes is incomplete, which results in depolarization of the ferroelectric.[7,8]

the total additional magnetization will be relatively small.[2] Therefore, using the ferromagnet/ferroelectric/normal metal configuration as in Fig. 1, an additional magnetization on the ferromagnet will not be compensated by electron depletion from the normal metal side.

If the normal metal electrode is assumed to be a perfect metal, then the bound charges are completely compensated by screening electrons. In this case, the depolarization effect on the ferroelectric can be ignored because the value will be very small since the density of screening electrons is the same as the density of bound charges. However, in the case of real metal, the compensation is not complete, and there is a depolarization field directed opposite to the polarization. Hence the depolarization field should be considered when calculating additional magnetization. In this case, the density of the screening electrons will be less than the density of bound charges.

The effect of incomplete compensation of screening electrons has been studied by Mehta[7] and Tilley.[8] In the Tilley model, the electric field in the electrode is calculated using the Thomas-Fermi approximation. The depolarization field can be derived by first expressing the total energy density of the system. This energy density consists of a ferroelectric in the field produced by the electrodes and can be written in dimensionless form as (see Appendix for details):

$$\frac{\tilde{F}}{S} = \int d\tilde{x}\left\{\left(\frac{T}{T_c}-1\right)\frac{\tilde{P}^2}{2}+\frac{\tilde{P}^4}{4}+\frac{1}{2}\left(\frac{d\tilde{P}}{d\tilde{x}}\right)^2+\frac{1}{2\epsilon_\circ\epsilon_f a_\circ T_c}\tilde{P}^2 + \frac{\tilde{V}_\circ}{\tilde{\alpha}+\tilde{l}}\tilde{P}\right\} - \frac{1}{2\epsilon_\circ\epsilon_f a_\circ T_c}\frac{1}{(\tilde{\alpha}+\tilde{l})}\left[\int \tilde{P}d\tilde{x}\right]^2 + \frac{\tilde{\gamma}}{8\epsilon_\circ(\tilde{\alpha}+\tilde{l})^2}\left(\frac{1}{a_\circ T_c}\right)\left[\int \tilde{P}d\tilde{x}\right]^2 - \frac{2\epsilon_f\tilde{V}_\circ\tilde{\gamma}}{8(\tilde{\alpha}+\tilde{l})^2} \times \int \tilde{P}d\tilde{x} + \left(\frac{a_\circ^2T_c^2}{K^{1/2}}\right)\frac{\epsilon_\circ\epsilon_f^2\tilde{\gamma}}{8(\tilde{\alpha}+\tilde{l})^2}\tilde{V}_\circ^2 + \frac{1}{2\tilde{\delta}}(P_+^2+P_-^2), \tag{1}$$

where the parameter γ is defined as

$$\gamma = \left(\frac{\lambda_l}{\epsilon_l}\beta_l + \frac{\lambda_r}{\epsilon_r}\beta_r\right) \quad \text{with} \quad \beta_{l,r} = \frac{\sinh\left(\frac{L-l}{\lambda_{l,r}}\right)-\left(\frac{L-l}{\lambda_{l,r}}\right)}{\sinh^2\left(\frac{L-l}{2\lambda_{l,r}}\right)}. \tag{2}$$

Here, $\epsilon_\circ$ is the vacuum permittivity, ϵ_f represents the permittivity of the ferroelectric, and ϵ_r and ϵ_l are the permittivities of the right and left electrodes. The parameters $a_\circ$, B, and K represent Ginzburg-Landau constants while the parameter δ represents the extrapolation length, which indicates that the polarization at the ferroelectric interface is different from the polarization in the interior of ferroelectric. The dimensionless polarization $\tilde{P}$ is related to the real polarization P as $P = P_\circ\tilde{P}$, where $P_\circ = \frac{a_\circ T_c}{B}$, with T_c denoting the Curie temperature. The other dimensionless parameters, such as dimensionless parameters for energy density ($\tilde{F}$), position ($\tilde{x}$), external voltage ($\tilde{V}_\circ$), and ferroelectric thickness ($\tilde{l}$), are defined by $\tilde{F} = \frac{B}{a_\circ^{3/2}T_c^{3/2}K^{1/2}}F$, $\tilde{x} = (\frac{a_\circ T_c}{K})^{1/2}x$, $\tilde{V}_\circ = (\frac{B}{K})^{1/2}\frac{V_\circ}{a_\circ T_c}$, and $\tilde{l} = (\frac{a_\circ T_c}{K})^{1/2}l$. The dimensionless parameters $\tilde{\alpha}$ and $\tilde{\gamma}$ are defined as $\tilde{\alpha} = (\frac{a_\circ T_c}{K})^{1/2}\alpha$ and $\tilde{\gamma} = (\frac{a_\circ T_c}{K})^{1/2}\gamma$, where α is

$$\alpha = \lambda_l\frac{\epsilon_f}{\epsilon_l}\frac{\cosh\left(\frac{L-l}{2\lambda_l}\right)-1}{\sinh\left(\frac{L-l}{2\lambda_l}\right)} + \lambda_r\frac{\epsilon_f}{\epsilon_r}\frac{\cosh\left(\frac{L-l}{2\lambda_r}\right)-1}{\sinh\left(\frac{L-l}{2\lambda_r}\right)}. \tag{3}$$

Here, λ_r and λ_l represent the screening lengths of the right and left electrodes.

The value of polarization P in thermal equilibrium is given by the minimum of energy density F in Eq. (1) as a function of P. The equilibrium polarization satisfies $\frac{dF}{dP} = 0$, yielding

$$\left(\frac{T}{T_c}-1\right)\tilde{P}+\tilde{P}^3-\left(\frac{\partial^2\tilde{P}}{\partial\tilde{x}}\right)+\frac{1}{\epsilon_f}\left(\frac{1}{a_\circ T_c}\right)[\tilde{P}-\eta\tilde{\bar{P}}]+\frac{\tilde{V}_\circ}{\tilde{l}}\eta = 0, \tag{4}$$

where $\eta = \frac{l}{\alpha+l} - \frac{\gamma l}{4(\alpha+l)^2}$. By comparing with the Kretschmer and Binder density energy for the ferroelectric with the perfectly conducting electrodes,[12] the third and fourth terms on the left-hand side of Eq. (4) are defined as the depolarization and external fields with the form

$$\tilde{E}_d = -\frac{1}{\epsilon_f}\left(\frac{1}{a_\circ T_c}\right)[\tilde{P}-\eta\tilde{\bar{P}}], \tag{5}$$

$$\tilde{E}_{\text{ext}} = -\frac{\tilde{V}_\circ}{\tilde{l}}\eta, \tag{6}$$

where the parameter η is defined as

$$\eta = \frac{l}{\alpha+l} - \frac{\gamma l}{4(\alpha+l)^2}. \tag{7}$$

In the limiting case of a perfect metal, the screening length $\lambda \to 0$, hence $\alpha \to 0$ and $\gamma \to 0$, so that $\eta \to 1$. This will result in expressions for the energy density and depolarization fields that are the same as in the Kretschmer and Binder system.[12] For a real metal, the value of η is always less than 1.

The parameter η in Eq. (7) is strongly dependent on the electrode thicknesses. For example, if the electrodes are much thicker than the screening length by at least an order of magnitude, $(L-l) \gg \lambda$, then β and $\gamma \to 0$ and $\alpha \sim \lambda\frac{\epsilon_f}{\epsilon_e}$. In this case, $\eta \sim \frac{l}{\alpha+l}$.

Parameter values for Fe and $BaTiO_3$ are given in Table I. Using these parameters, η is calculated as a function of ferroelectric thickness l and the results are shown in Fig. 2(a). We see that η increases with increasing ferroelectric thickness and approaches unity in the limit $l \gg \alpha$. The value of α is dependent on the thickness of the ferromagnet. In the case in which the ferromagnet thickness is much bigger than the screening length of the electrode, $L-l \gg \lambda$, and the value of α saturates at 250 nm. In this limit, the value of η will approach

TABLE I. Parameter values of Fe and $BaTiO_3$ used in the numerical calculations. The parameter values for Fe are taken from Refs. 4,9, and 10, while parameter values for $BaTiO_3$ are taken from Ref. 11.

Fe	Value	$BaTiO_3$	Value
$\rho^{\uparrow}$	$0.87\ \text{eV}^{-1}\ \text{nm}^{-3}$	$a_\circ$	$6.65 \times 10^5\ \text{V m C}^{-1}\ \text{K}^{-1}$
$\rho^{\downarrow}$	$0.24\ \text{eV}^{-1}\ \text{nm}^{-3}$	T_c	391 K
J	2.4 eV nm^3	ϵ_f	10^3
λ	1.3 Å	B	$3.56 \times 10^9\ \text{V m}^5\ \text{C}^{-3}$
M_s	1.67×10^6 A/m	K	$4.51 \times 10^{-9}\ \text{V m}^3\ \text{C}^{-1}$
H_a	3.98×10^4 A/m		

1 if the ferroelectric thickness is larger than 10^3 nm. Since the ferromagnet thicknesses 5 nm and 10 nm produce almost the same value of α, then both thicknesses yield approximately the same values for η. Note that η is an order of magnitude smaller for ferroelectric thicknesses below 100 nm. In this limit, the depolarization field becomes important. The depolarization is very small and can be neglected when the thickness of the ferroelectric is around 1 μm. We note that the use of a thick ferroelectric decreases the effective magnetic susceptibility of the overall system.

We find that an FE thickness of 500 nm produces an optimal balance between sensitivity to electric fields and strength of ferromagnetic response with these parameters. For this thickness, η is only 0.67 and there are significant depolarization fields. This increases the magnitude of the applied electric field needed to create a large polarization. The polarization is also nonuniform due to surface effects. An example polarization profile is shown in Fig. 2(b). At $E_{\text{ext}} = 1 \times 10^7$ V/m^2, the average polarization $\bar{P} = 0.128$ C/m^2.

III. ADDITIONAL MAGNETIZATION

We now calculate the additional interface magnetization induced by the ferroelectric polarization. The screening charge is present over several ferromagnetic layers at the interface with an exponential decrease in charge density away from the interface on the ferromagnet side.[5] According to Zhang,[4] the total charge density in the metallic magnet is the sum of two spin populations defined such that $n(x) = n^{\uparrow}(x) + n^{\downarrow}(x)$. The

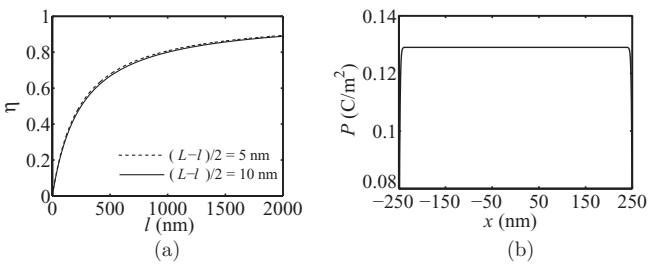

FIG. 2. In (a), values of η as a function of FE thickness are shown, and in (b) the polarization profile is given with the magnetic electrode thickness $(L - l)/2 = 20$ nm and the FE thickness $l = 500$ nm. Parameters are appropriate to Fe and $BaTiO_3$.

induced charge creates an additional spin-dependent potential defined as[5]

$$e\delta V^{\sigma} = eV_c(x) + J[\delta n^{\sigma}(x) - \delta n^{-\sigma}(x)], \tag{8}$$

where V_c is the Coulombic potential, which satisfies Poisson's equation:

$$\frac{d^2V_c(x)}{dx^2} = -\frac{e}{\epsilon_\circ}[\delta n^{\sigma}(x) + \delta n^{-\sigma}(x)]. \tag{9}$$

The second term on the right-hand side of Eq. (8) is associated with an additional exchange potential where J represents the exchange splitting constant between two spin states. The induced charge density is estimated using the Thomas-Fermi approximation, where the induced charge density $\delta n^{\sigma}(x)$ is related to a small change in potential $\delta V^{\sigma}(x)$ via

$$n^{\sigma}(x) + \delta n^{\sigma}(x) = \frac{(2S+1)}{6\pi^2\hbar^3}\{2m[\mu - eV^{\sigma}(x) - e\delta V^{\sigma}(x)]\}^{3/2}, \tag{10}$$

where μ represents chemical potential. Assuming that $\delta V^{\sigma}(x)$ is small, then the induced charge density can be calculated using a Taylor expansion. Taking the first-order term, we find

$$\delta n^{\sigma}(x) = \frac{\partial n^{\sigma}(x)}{\partial V^{\sigma}(x)}\delta V^{\sigma}(x), \tag{11}$$

where

$$\frac{\partial n^{\sigma}(x)}{\partial V^{\sigma}(x)} = -\frac{(2S+1)}{4\pi^2\hbar^3}(2m)^{3/2}[\mu - V^{\sigma}(x)]^{1/2} = -e\rho^{\sigma} \tag{12}$$

with ρ^{σ} as the spin-dependent density of states at the Fermi level. Using Eqs. (8) and (11), we obtain the relation[4]

$$\delta n^{\uparrow}(x) - \delta n^{\downarrow}(x) = -\frac{\rho^{\uparrow} - \rho^{\downarrow}}{1 + J(\rho^{\uparrow} + \rho^{\downarrow})}eV_c(x). \tag{13}$$

The local induced magnetization is found from $\delta M(x) = [\delta^{\uparrow}n(x) - \delta^{\downarrow}n(x)]\mu_B$. The spin-dependent potential is then calculated by using Eqs. (11) and (9). The result is

$$\frac{d^2V_c(x)}{dx^2} = \frac{V_c(x)}{\lambda^2}, \tag{14}$$

where λ is a screening length defined by

$$\lambda = \left[\frac{e^2}{\epsilon_\circ}\frac{\rho^{\uparrow} + \rho^{\downarrow} + 4J\rho^{\uparrow}\rho^{\downarrow}}{1 + J(\rho^{\uparrow} + \rho^{\downarrow})}\right]^{-1/2}. \tag{15}$$

The Coulomb potential in the electrode obeys the boundary condition

$$V_c\left(\frac{\pm l}{2}\right) = V^{\circ}_{r,l} \quad \text{and} \quad V_c\left(\frac{\pm L}{2}\right) = 0, \tag{16}$$

leading to a solution of the form

$$V_c(x) = V_l^{\circ}\exp\left(\frac{\frac{1}{2}l + x}{\lambda_l}\right) \quad \text{for} \quad x < \frac{-l}{2},$$
$$V_c(x) = V_r^{\circ}\exp\left(\frac{\frac{1}{2}l - x}{\lambda_r}\right) \quad \text{for} \quad x > \frac{l}{2}. \tag{17}$$

The amplitude of the potential $V^{\circ}_{l,r}$ is found by imposing charge conservation:

$$\sigma = \frac{1}{4\pi}\int_{-\infty}^{-l/2}\left[\frac{\partial^2 V}{\partial x^2}\right]dx = -\frac{1}{4\pi}\int_{l/2}^{\infty}\left[\frac{\partial^2 V}{\partial x^2}\right]dx. \quad (18)$$

The result is

$$V^{\circ}_{r,l} = \pm\frac{\sigma\lambda_{l,r}}{\epsilon_{\circ}}. \quad (19)$$

An expression for the local additional magnetization is finally obtained from Eqs. (19), (13), and (17) as[5]

$$\delta M(x) = -\frac{(\rho^{\uparrow}-\rho^{\downarrow})\mu_B}{1+J(\rho^{\uparrow}+\rho^{\downarrow})}eV_c(x). \quad (20)$$

The induced local magnetization is largest at the interface ($x = -l/2$) and decreases exponentially as it goes into the ferromagnet. The total additional magnetization (in μ_B per area) is obtained by integrating the induced local magnetization in Eq. (20) over the ferromagnet layer:

$$\Delta M = -\frac{\sigma}{e}\frac{(\rho^{\uparrow}-\rho^{\downarrow})\mu_B}{\rho^{\uparrow}+\rho^{\downarrow}+4J\rho^{\uparrow}\rho^{\downarrow}}. \quad (21)$$

The associated field is $\mu_{\circ}\Delta M/\lambda$.

Using the parameters for Fe and $BaTiO_3$ given in Table I, the additional magnetization ΔM was calculated for a 500-nm-thick ferroelectric with a ferromagnet and a normal metal each 20 nm thick. The increase in external field will increase the polarization, thereby increasing the density of bound charges. The bound charge is compensated by the screening charges, which increase the additional magnetization via a polarization factor related to the *s*-*d* coupling and the exchange interaction in the ferromagnet. Results calculated under the assumptions and approximations outlined above are shown in Fig. 3(a). For example, when the external field is set at 3.7% of the breakdown field, the average polarization will be 0.077 C/m^2, which in turn generates $\sigma = -0.0575$ C/m^2 of screening charge. The magnetization is enhanced by 0.4% (5.17×10^3 A/m) relative to the lattice magnetization M_s. The magnetization enhancement is shown in Fig. 3(a) for variations of the external field from 3.7% to 74%, resulting in an enhanced magnetization varying from 0.4% to 1.2%.

As discussed earlier, the thickness of the ferroelectric influences the magnitude of polarization, with an increase of the ferroelectric film thickness resulting in an increased polarization. Shown in Fig. 3(b) are results for the corresponding enhancement in magnetization. The external field is set at 44% of the breakdown field and the ferroelectric film thickness is varied from 100 to 700 nm. This causes the polarization to vary from 0.059 to 0.134 C/m^2, causing the additional magnetization to vary from 0.3% to 0.74%.

The thickness of the ferromagnet influences the additional magnetization according to the parameter α, as in Eq. (A9). This in turn changes the depolarization field through parameter η. As can be seen in Fig. 2(a), α saturates as the ferromagnet thickness increases. For the parameters used here, the additional magnetization is independent of ferromagnet thickness for ferromagnet thicknesses greater than 1 nm.

We now calculate and compare the additional magnetization for different metallic ferromagnets. In particular, we show results for the half metal CrO_2, the Heusler alloy (Co_2MnGe),

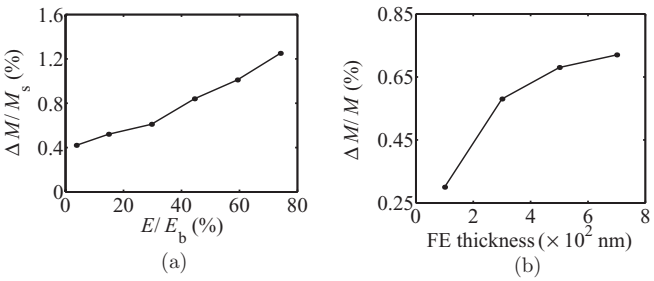

FIG. 3. In (a), the additional magnetization is shown for a range of applied electric fields, while in (b) the effect of FE thickness on additional magnetization is shown. Parameters appropriate to Fe and $BaTiO_3$ are assumed.

and also permalloy ($Fe_{0.8}Ni_{0.2}$). The assumed parameters are given in Table II.

Results for the additional magnetization for these different metallic ferromagnets are shown in Fig. 4(a). The results depend strongly on the density of states at the Fermi level ($\Delta\rho = \rho^{\uparrow} - \rho^{\downarrow}$) and the exchange splitting J. Since the half metal only has one type of spin-dependent density of states at the Fermi level, it has the largest value of $\Delta\rho$. Since the half metal has only one type of spin state at the Fermi level, and all the screening charges are polarized in one direction, where the polarized ratio $\frac{\rho^{\uparrow}-\rho^{\downarrow}}{\rho^{\uparrow}+\rho^{\downarrow}} = 1$, the additional magnetization in Eq. (21) becomes that of a half metal, $\Delta M = -\frac{\sigma}{e}\mu_b$, independent of the density of states. Since screening charges show only small differences between various half metal materials,[23] the additional magnetization in μ_b/nm^2 will be similar to that shown in Fig. 4(a). Permalloy has a larger polarized ratio compared to iron (0.63 as opposed to 0.57), so the additional magnetizations for both materials are located below the half metal curve. The additional magnetization of permalloy is higher than that of Fe.

The additional magnetizations in terms of percentage relative to the lattice magnetization M_s are shown in Fig. 4(b). The Heusler alloy has a value of ΔM, in μ_b/nm^2, similar to that of CrO_2. Nevertheless, the Heusler alloy has a lattice magnetization that is twice the size of that in CrO_2. As a consequence, the percentage ΔM in a Heusler alloy is smaller than that for CrO_2. Iron has the smallest additional

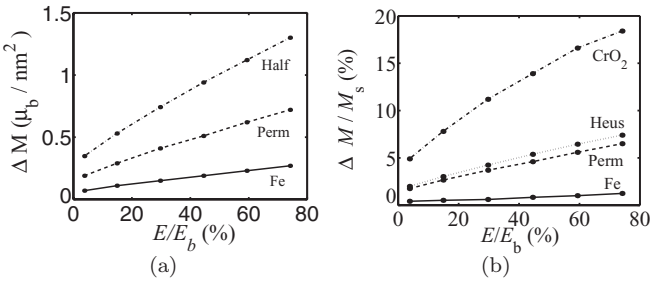

FIG. 4. The additional magnetization in a FM/FE/NM trilayer system for four different FM electrode materials. In (a), the additional magnetization is presented in units of μ_b/nm^2 while in (b) the percentage relative to the lattice magnetization is shown. The dotted line ("Heus") represents a system with Heusler alloy Co_2MnGe as the FM electrode. The solid line indicates Fe and the dashed-dot and dashed lines are for CrO_2 and permalloy, respectively.

TABLE II. Parameter values for metallic ferromagnet CrO_2, Co_2MnGe, and permalloy. The parameters for CrO_2 are taken from Refs. 5 and 13–16, values for Co_2MnGe are taken from Refs. 17–20, and parameters for permalloy are approximated from Refs. 21 and 22.

Material	$\rho^{\uparrow}$	$\rho^{\downarrow}$	J	λ	M_s	H_a
CrO_2	0.69 eV^{-1} nm^{-3}	0	1.8 eV nm^3	1.7 Å	4.71×10^5 A/m	6.05×10^3 A/m
Co_2MnGe	1.5 eV^{-1} nm^{-3}	0	1 eV nm^3	1.5 Å	9.5×10^5 A/m	3.98×10^2 A/m
Permalloy	0.25 eV^{-1} nm^{-3}	1.1 eV^{-1} nm^{-3}	0.27 eV nm^3	1.2 Å	8.59×10^5 A/m	2.22×10^3 A/m

magnetization of all, but it also has the largest magnetization M_s. This results in the smallest value of relative ΔM among the other electrodes.

IV. EFFECTIVE MEDIUM: SUSCEPTIBILITY AND SPIN WAVES

The effective-medium approximation is used to account for dipolar contributions to the spin wave frequencies.[24–28] Conventional effective-medium theory assumes that parameters across the layer are constant. This is not true for the thicknesses of films of interest since there is additional magnetization at the ferromagnet/ferroelectric interface, hence an entire-cell version of the effective-medium theory is used. The entire-cell effective-medium theory divides each film into layers thin enough that an effective-medium approach can be taken for fields across each interface.[26,27] A sketch of this film subdivision is shown in Fig. 5. Suppose the normal metal film is comprised of layer $N = 1$ to $N_{\rm I}$, the layers $N_{\rm I} + 1$ to $N_{\rm II}$ are inside ferroelectric film, and the layers $N_{\rm II} + 1$ to $N_{\rm III}$ are inside ferromagnet film. The Maxwell boundary conditions are applied at each interface, and the average of the dynamic magnetization components **m** and dipolar fields **h** is found. Components of the dynamic susceptibility are then calculated.

We first derive equations of motion for each layer i using the nondissipative torque equation

$$\frac{1}{\gamma}\frac{\partial \mathbf{M_i}}{\partial t} = \mu_\circ \mathbf{M_i} \times \left(\mathbf{H_i^{eff}} + \mathbf{H_i^{ex}}\right). \tag{22}$$

Here $\mathbf{H_i^{eff}}$ represents an effective field for layer i, which consists of an in-plane anisotropy field $H_a\hat{z}$, an out-of-plane anisotropy $H_u\hat{x}$, the external magnetic field $H_\circ\hat{z}$, and a dipolar field **h**. An exchange field is represented by $\mathbf{H_{ex}}$. The magnetization for layer i is represented by M_i. In this layered system, the interlattice distance in the $\hat{x}$ direction is denoted by Δ_x, which is similar to the spacing in the previous calculation of polarization. The exchange field at lattice i for the discrete system can be written as

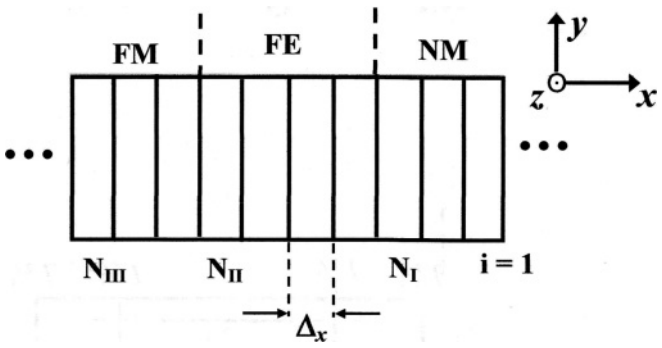

FIG. 5. The geometry used for application of the entire-cell effective-medium method. Each film of the trilayer system is subdivided into thin layers with the thickness of sublayer denoted as Δ_x. Layers $N = 1$ to $N_{\rm I}$ are inside NM, layers $N_{\rm I} + 1$ to $N_{\rm II}$ are inside FE, and layers $N_{\rm II} + 1$ to $N_{\rm III}$ are inside FM.

$$\mathbf{H_i^{ex}} = \frac{2A}{\mu_\circ M_s^2}\left[\frac{\mathbf{M_{i+1}} + \mathbf{M_{i-1}} - 2\mathbf{M_i}}{\Delta_x^2}\right], \tag{23}$$

where A represents the stiffness exchange constant.

We define the magnetization as

$$\mathbf{M_i} = \left(m_i^x, m_i^y, M_s\right), \tag{24}$$

where m_i represents the dynamic term such that $m_i \ll M_s$. The equations of motion after linearization and assuming $m_i \propto e^{i\omega t}$ are

$$-i\frac{\omega}{\gamma}m_i^x = \mu_\circ(H_\circ + H_a)m_i^y - \frac{2A}{M_s}\frac{\left(m_{i+1}^y + m_{i-1}^y - 2m_i^y\right)}{\Delta_x^2} - \mu_\circ M_s h_y, \tag{25a}$$

$$-i\frac{\omega}{\gamma}m_i^y = -\mu_\circ(H_\circ + H_a + H_u)m_i^x + \frac{2A}{M_s}\frac{\left(m_{i+1}^x + m_{i-1}^x - 2m_i^x\right)}{\Delta_x^2} + \mu_\circ M_s h_x. \tag{25b}$$

In the next step, we require the dipolar field to obey Maxwell's boundary conditions. These are the continuity of tangential **h** and the continuity of normal **b** across each layer interface. We write these as

$$h_i^y = h_{i+1}^y = \cdots = h_N^y = C_y, \tag{26a}$$

$$h_i^x + m_i^x = h_{i+1}^x + m_{i+1}^x = \cdots = h_N^x + m_N^x = C_x, \tag{26b}$$

where C_y and C_x are constant. Requiring continuities of the tangential **h** and normal **b** fields in Eq. (26), the equation of motion can be written as

$$-i\frac{\omega}{\gamma}m_i^x = \mu_\circ(H_\circ + H_a)m_i^y - \frac{2A}{M_s}\frac{\left(m_{i+1}^y + m_{i-1}^y - 2m_i^y\right)}{\Delta_x^2} - \mu_\circ M_s C_y, \tag{27}$$

$$-i\frac{\omega}{\gamma}m_i^y = -\mu_\circ(H_\circ + H_a + H_u + M_s)m_i^x + \frac{2A}{M_s}\frac{\left(m_{i+1}^x + m_{i-1}^x - 2m_i^x\right)}{\Delta_x^2} + \mu_\circ M_s C_x. \tag{28}$$

Note that continuity of normal **h** gives rise to a demagnetization term $\mu_\circ M_s$ in the equations of motion on account of interfaces where M_s changes.

A. Spin waves

We now employ the equations of motion Eqs. (27) and (28) to study the influence of the additional magnetization on the modes of spin waves (i.e., the spin wave resonances). It is necessary to derive additional boundary conditions at the ferroelectric/ferromagnet interface and the ferromagnet/normal metal interface to take into account exchange between magnetic layers. We begin by defining the equation of motion with surface anisotropy:[29]

$$\frac{1}{\gamma}\frac{\partial \mathbf{M}}{\partial t} + \mu_\circ \mathbf{M} \times \mathbf{H}_{\text{eff}} + \frac{2A}{M_s^2}\mathbf{M} \times \nabla^2 \mathbf{M} + \mu_\circ \mathbf{M} \times \mathbf{H}_s = \mathbf{0}. \tag{29}$$

Here $\mathbf{H_s}$ is the surface anisotropy field defined as $\mathbf{H_s} = \frac{2K_s}{\mu_\circ M_s^2} M_x \hat{x}$, with K_s being the surface anisotropy constant. The effective field H_{eff} represents the external applied and uniaxial anisotropy effective fields. Integrating the equation of motion over the volume around the surface yields the Rado-Weertman boundary condition[29]

$$\frac{2A}{M_s^2}\mathbf{M} \times \frac{\partial \mathbf{M}}{\partial x} + \frac{2K_s}{M_s^2} M_x \hat{x} \times \mathbf{M} = \mathbf{0}. \tag{30}$$

There is an additional boundary condition at the ferroelectric/ferromagnet interface (layer $N_{\text{II}} + 1$) because there is an additional magnetization ΔM that affects the condition at the interface. As discussed earlier, the additional magnetization is largely confined close to the interface. Here we assume that it exists only in the first layer of the ferromagnet near the ferromagnet/ferroelectric interface (layer $N_{\text{II}} + 1$). The additional boundary condition, from Eq. (30), is

$$M_s \frac{\partial m_y}{\partial x} - m_y \frac{\partial M_s}{\partial x} = 0, \tag{31a}$$

$$M_s \frac{\partial m_x}{\partial x} - \left(\zeta M_s + \frac{\partial M_s}{\partial x}\right) m_x = 0, \tag{31b}$$

where $\zeta = K_s/A$. The above boundary condition can be approximated by assuming $\frac{\partial M_s}{\partial x} \approx \frac{M^s_{N_{\text{II}}+2} - M^s_{N_{\text{II}}+1}}{\Delta_x} = -\frac{\Delta M}{\Delta_x}$, where $M^s_{N_{\text{II}}+1}$ represents the layer magnetization at the ferroelectric/ferromagnet interface with additional magnetization ΔM from Eq. (21), while $M^s_{N_{\text{II}}+2} = M_s$ represents the magnetization at the noninterface layer inside the ferromagnet and without any additional magnetization. This allows the boundary condition to be written as

$$\frac{\partial m_y}{\partial x} + m_y \frac{\Delta M}{M_s \Delta_x} = 0, \tag{32a}$$

$$\frac{\partial m_x}{\partial x} - \left(\zeta - \frac{\Delta M}{M_s \Delta_x}\right) m_x = 0. \tag{32b}$$

Since both the normal metal and the ferroelectric are nonmagnetic material, the magnetization of the layers inside both the normal metal and the ferroelectric are considered to be zero. However, to be able to derive the magnetic boundary condition at the ferromagnet/ferroelectric interface (layer $N_{\text{II}} + 1$), we assumed the layer N_{II} in ferroelectric as an imaginary layer. Hence, the boundary condition in Eqs. (32a) and (32b) for layer $N_{\text{II}} + 1$ at the ferroelectric/ferromagnet interface can be written in the discrete form as

$$\frac{m^y_{N_{\text{II}}+2} - m^y_{N_{\text{II}}}}{2\Delta_x} + \frac{\Delta M}{M_s \Delta_x} m^y_{N_{\text{II}}+1} = 0, \tag{33a}$$

$$\frac{m^x_{N_{\text{II}}+2} - m^x_{N_{\text{II}}}}{2\Delta_x} - \left(\zeta - \frac{\Delta M}{M_s \Delta_x}\right) m^x_{N_{\text{II}}+1} = 0. \tag{33b}$$

Substitution of Eq. (33) into the discrete second derivative form of the exchange field yields the boundary components on the additional magnetization for the ferromagnet/ferroelectric interface (layer $N_{\text{II}} + 1$) as

$$\nabla^2 m^y_{N_{\text{II}}+1} = \frac{2m^y_{N_{\text{II}}+2} - 2\left(1 - \frac{\Delta M}{M_s}\right) m^y_{N_{\text{II}}+1}}{\Delta_x^2}, \tag{34a}$$

$$\nabla^2 m^x_{N_{\text{II}}+1} = \frac{2m^x_{N_{\text{II}}+2} - 2\left(1 + \zeta\Delta_x - \frac{\Delta M}{M_s}\right) m^x_{N_{\text{II}}+1}}{\Delta_x^2}. \tag{34b}$$

A similar procedure is performed for the ferromagnet/normal metal interface (layer N_{III}) by setting the additional magnetization to zero ($\Delta M = 0$). The result is

$$\nabla^2 m^y_{N_{\text{III}}} = \frac{2m^y_{N_{\text{III}}-1} - 2m^y_{N_{\text{III}}}}{\Delta_x^2}, \tag{35a}$$

$$\nabla^2 m^x_{N_{\text{III}}} = \frac{2m^x_{N_{\text{III}}-1} - 2\left(1 + \zeta\Delta_x\right) m^x_{N_{\text{III}}}}{\Delta_x^2}. \tag{35b}$$

Next, we use the boundary conditions Eqs. (34) and (35) together with the equations of motion from Eq. (27) to obtain the mode frequencies and profiles. We approximate the dynamic terms by setting the constant terms (C_x, C_y) to zero. As a consequence, the driving fields are set at $h_y = 0$ and $h_x \neq 0$ (in this case, $h_x = -m_x$). Hence, the different phase between the oscillation of the magnetization component m_x and the driving field h_x is π. We admit that the approximation in this problem is crude, however this approximation is very useful since we can calculate the dynamic magnetization easily. Using the approximation, the equations of motion can be brought into the form of an eigenvalue problem. Explicitly, one has

$$-i\frac{\omega}{\gamma} m^x_i = \mu_\circ (H_\circ + H_a) m^y_i - \frac{2A}{M_s}\frac{\left(m^y_{i+1} + m^y_{i-1} - 2m^y_i\right)}{\Delta_x^2}, \tag{36a}$$

$$-i\frac{\omega}{\gamma} m^y_i = -\mu_\circ (H_\circ + H_a + H_u + M_s) m^x_i + \frac{2A}{M_s}\frac{\left(m^x_{i+1} + m^x_{i-1} - 2m^x_i\right)}{\Delta_x^2}, \tag{36b}$$

with the equation for layer $N_{\text{II}} + 1$ near the ferroelectric/ferromagnet interface given by

$$-i\frac{\omega}{\gamma} m^x_{N_{\text{II}}+1} = \mu_\circ \left[(H_\circ + H_a) + 2\kappa\left(1 - \Delta M/M_s\right)\right] m^y_{N_{\text{II}}+2} - 2\kappa\mu_\circ m^y_{N_{\text{II}}+1}, \tag{37a}$$

$$-i\frac{\omega}{\gamma} m^y_{N_{\text{II}}+1} = -\mu_\circ [(H_\circ + H_a + H_u + M_s) + 2\kappa(1 + \zeta\Delta_x - \Delta M/M_s)] m^x_{N_{\text{II}}+2} + 2\kappa\mu_\circ m^x_{N_{\text{II}}+1}, \tag{37b}$$

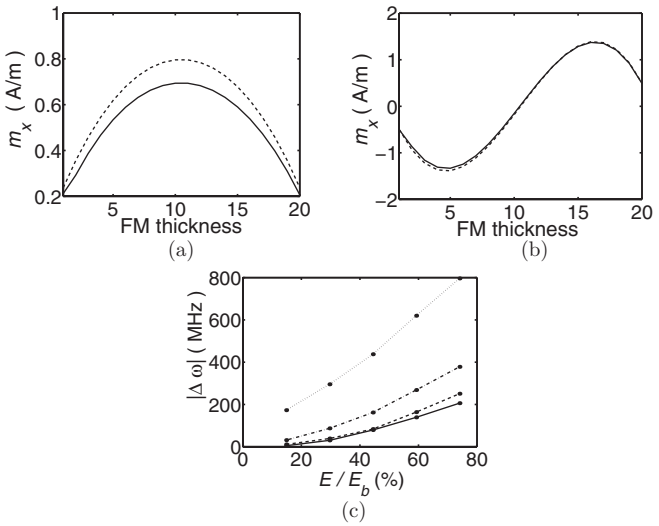

FIG. 6. Profile of m_x for the FMR and first excited standing spin wave mode. Solid lines represent the case of additional magnetization at the surface layer, and dashed lines represent the situation without an additional magnetization. The profile for the FMR is presented in (a), and the profile for first excited standing spin wave mode is illustrated in (b). In (c), the frequency shift is given for several modes. The solid line represents the FMR mode, the dashed line represents the first excited mode, the dashed-dotted line represents second excited mode, and the dotted line represents the third excited mode. Here, the parameter ω represents angular frequency.

and the equation for layer $N_{\rm III}$ at the ferromagnet/normal metal interface of the form

$$-i\frac{\omega}{\gamma}m^x_{N_{\rm III}} = \mu_\circ\left[(H_\circ + H_a) + 2\kappa\right]m^y_{N_{\rm III}-1} - 2\kappa\mu_\circ m^y_{N_{\rm III}}, \tag{38a}$$

$$-i\frac{\omega}{\gamma}m^y_{N_{\rm III}} = -\mu_\circ[(H_\circ + H_a + H_u + M_s) + 2\kappa(1+\zeta\Delta_x)]m^x_{N_{\rm III}-1} + 2\kappa\mu_\circ m^x_{N_{\rm III}}, \tag{38b}$$

where $\kappa = \frac{2A}{\mu_\circ M_s \Delta_x^2}$.

Results are presented in Fig. 6(a) for the FMR mode and Fig. 6(b) for the first excited spin wave mode. The external electric field is set at 29.6% of the breakdown field, giving rise to an additional magnetization of 8.1% relative to M_s. It can be seen that the additional magnetization has the smallest influence on the FMR profile, with a corresponding downshift of the resonance frequency $\Delta\omega = 30.16$ MHz.

The downshift on the first excited mode is $\Delta\omega = 38.76$ MHz. The value of $\frac{\Delta M}{M_s}$ is one order of magnitude lower than the pinning factor $\zeta\Delta_x$ (around 0.53), and according to Eq. (IV A) it decreases the effect of pinning. The decrease of pinning will increase the wavelength of spin waves, and thereby decrease the frequency. We also present the frequency shifts of several modes at different applied electric fields [see Fig. 6(c)]. It can be seen that the frequency shift increases with decreasing wavelength of the excited modes. The largest frequency shifts occur for the highest-order standing spin wave excitations.

B. Susceptibilities

We now calculate susceptibilities in the effective-medium approximation. We do this by writing the equations of motion from Eqs. (27) and (28) for the layer at the ferroelectric/ferromagnet interface as

$$(i\omega/\gamma)\,m_i^x + \mu_\circ(H_o + H_a)\,m_i^y = \mu_\circ(M_s + \Delta M_i)\,C_y, \tag{39a}$$

$$(i\omega/\gamma)\,m_i^y - \mu_\circ(H_o + H_a + H_u + M_i)\,m_i^x = -\mu_\circ(M_s + \Delta M_i)\,C_x. \tag{39b}$$

In this approximation, the other layers in the ferromagnet have a similar form but without ΔM. It should be noted that the layers at the ferroelectric and normal metal interfaces do not have magnetization, i.e., $m_i = 0$. However, both normal and tangential components of the dipolar field **h** exist and must satisfy the Maxwell boundary conditions for normal **b** and tangential **h**. We solve simultaneously the coupled set of equations of motion by fixing values of C_x and C_y (for example, $C_x = 1$ and $C_y = 2$) to obtain the set of m_i^x, m_i^y, h_i^x, and h_i^y averaged over all layers in the system, such as $\langle m_x\rangle = \frac{\sum_{i=1}^N m_i^x}{N}$. We therefore arrive at values for $\{\langle m^x\rangle, \langle m^y\rangle, \langle h^x\rangle, \langle h^y\rangle\}$.

The susceptibility components are defined through the relations $\langle m\rangle$ and dipolar field $\langle h\rangle$ by

$$\langle m_x\rangle = \chi_{xx}\langle h_x\rangle + \chi_{xy}\langle h_y\rangle, \tag{40a}$$

$$\langle m_y\rangle = \chi_{yy}\langle h_y\rangle + \chi_{yx}\langle h_x\rangle. \tag{40b}$$

Calculation of the susceptibility components requires $\{\langle m^x\rangle, \langle m^y\rangle, \langle h^x\rangle, \langle h^y\rangle\}$ to be determined from $\{C_x, C_y\}$ and will be a function of frequency ω. The susceptibility for the geometry given in Fig. 1 has the form

$$\chi = \begin{pmatrix} \chi_{xx} & i\chi_{xy} & 0 \\ -i\chi_{xy} & \chi_{yy} & 0 \\ 0 & 0 & 0 \end{pmatrix}. \tag{41}$$

Mode frequencies are obtained from the poles of the susceptibilities. Results from numerical calculations of the susceptibilities are shown in Fig. 7(a) for the following parameter values. The ferromagnet and normal metal layer are sliced into 20 layers, each with a thickness of 20 nm. The ferroelectric layer is divided into 500 layers with 1-nm-thick slices. For these materials, an external electric field 44% of the breakdown field gives an average polarization of 0.128 C/m^2.

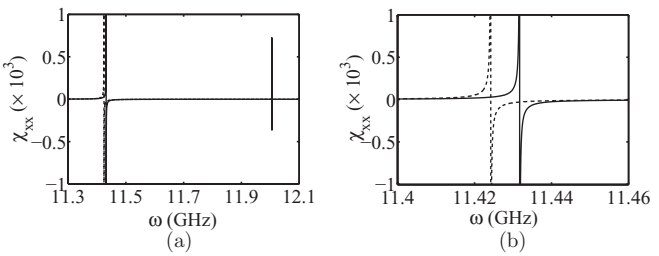

FIG. 7. Influence of the additional magnetization on the FMR frequency in trilayer unit cell. Iron is used as metallic ferromagnet. In (a), the additional magnetization generates an additional mode and shifts the original resonance frequency up, as illustrated in (b). The solid lines represent the case with additional magnetization, while the dashed line represents the case without additional magnetization.

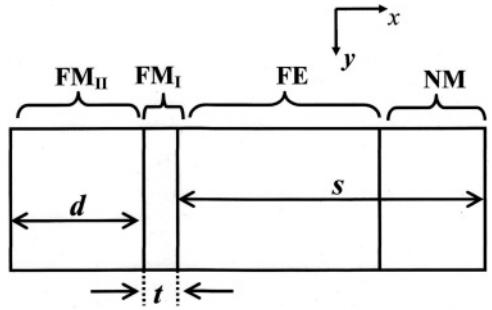

FIG. 8. Resonance modes for the perturbed thin film are approximated by a thin layer (FM_I) with thickness t exchange coupled to another layer FM_{II} layer with thickness d. The ratio of the thickness is similar to the ratio of the layers in the entire-cell model.

This value will result in an additional magnetization at the ferromagnet/ferroelectric interface of 4.6% the magnetization of permalloy. The solid line shows the susceptibility curve with additional magnetization accumulated at the surface layer, while the dashed line represents the susceptibility curve without additional magnetization.

In addition to the FMR mode at 11.4 GHz, an additional pole appears at around 12 GHz. There is also an upshift of the FMR frequency of around 7 MHz due to the additional magnetization. The appearance of this additional mode can be expected due to the strong localization of the additional magnetization. A new mode appears because the film has two magnetizations: M_s and $\tilde{M}_s = M_s + \Delta M$. This results in a mode mostly associated with the FMR mode of the perfect film and a localized mode largely confined to the perturbed layer.

We can derive analytically an expression for this new mode by approximating the system as composed of two coupled layers of unequal thickness and magnetization. One has magnetization $\tilde{M}_s = M_s + \Delta M$ with thickness t and the other has magnetization M_s with thickness d, where $d > t$ as illustrated in Fig. 8. Since the ferroelectric and normal metal do not have magnetization, we treat them as a spacer with thickness s.

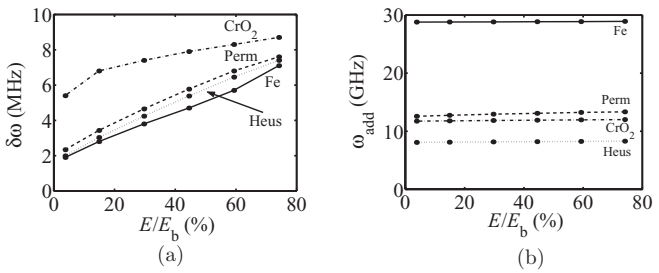

FIG. 9. Comparison of the frequency shift for the FMR mode (a) and the additional weak resonance (b) for Fe, permalloy, and half metal CrO_2 and Co_2MnGe values. The solid line represents Fe, the dashed line represents permalloy, and the dashed-dotted line represents CrO_2. The dotted line represents Co_2MnGe. Here, ω represents angular frequency.

For the ferromagnet layer with an additional magnetization, the equations of motion are

$$-\frac{i\omega}{\gamma}\tilde{m}_x = \mu_\circ H_{\rm eff}\tilde{m}_y - \mu_\circ C_y\tilde{M}_s, \tag{42a}$$

$$-\frac{i\omega}{\gamma}\tilde{m}_y = -\mu_\circ(H_{\rm eff} + \tilde{M}_s) + \mu_\circ C_x\tilde{M}_s, \tag{42b}$$

and the equations of motion for ferromagnet layers without additional magnetization are

$$-\frac{i\omega}{\gamma}m_x = \mu_\circ H_{\rm eff}m_y - \mu_\circ C_y M_s, \tag{43a}$$

$$-\frac{i\omega}{\gamma}m_y = -\mu_\circ(H_{\rm eff} + M_s)m_x + \mu_\circ C_y M_s, \tag{43b}$$

where $H_{\rm eff} = H_\circ + H_a$. Setting $C_y = 0$, the solution of $\tilde{m}_x$ and $\tilde{h}_x$ for the thin ferromagnet which possesses additional magnetization ΔM is

$$\tilde{m}_x = \frac{\mu_\circ^2 H_{\rm eff}\tilde{M}_s C_x}{\left[\mu_\circ^2 H_{\rm eff}(H_{\rm eff} + \tilde{M}_s) - \frac{\omega^2}{\gamma^2}\right]}, \tag{44a}$$

$$\tilde{h}_x = \frac{\left(\mu_\circ^2 H_{\rm eff}^2 - \frac{\omega^2}{\gamma^2}\right)C_x}{\left[\mu_\circ^2 H_{\rm eff}(H_{\rm eff} + \tilde{M}_s) - \frac{\omega^2}{\gamma^2}\right]}, \tag{44b}$$

and the solution for the ferromagnet layer without ΔM (the thick layer) is

$$m_x = \frac{\mu_\circ^2 H_{\rm eff}M_s C_x}{\left[\mu_\circ^2 H_{\rm eff}(H_{\rm eff} + M_s) - \frac{\omega^2}{\gamma^2}\right]}, \tag{45a}$$

$$h_x = \frac{\left(\mu_\circ^2 H_{\rm eff}^2 - \frac{\omega^2}{\gamma^2}\right)C_x}{\left[\mu_\circ^2 H_{\rm eff}(H_{\rm eff} + M_s) - \frac{\omega^2}{\gamma^2}\right]}. \tag{45b}$$

Since the magnetization of the normal metal and ferroelectric are zero, the magnetic field inside these layers is $h_x = C_x$. The effective susceptibility components can be defined as

$$\chi_{xx} = \frac{t\tilde{m}_x + dm_x}{t\tilde{h}_x + dh_x + sC_x}. \tag{46}$$

We substitute Eqs. (44a) and (45a) into the expression for the susceptibility, resulting in components that share a common denominator. Setting the denominator to zero, we arrive at

$$\tilde{\omega}^4 - B\tilde{\omega}^2 + C = 0, \tag{47}$$

where

$$B = \frac{t+d}{T}\mu_\circ^2\left(H_{\rm eff}^2 + \alpha_h\right) + \frac{d+s}{T}\mu_\circ^2 H_{\rm eff}\mu_\circ\Delta M + 2\frac{s}{T}\mu_\circ^2\alpha_h, \tag{48a}$$

$$C = \frac{t+d}{T}\mu_\circ^4 H_{\rm eff}^2\alpha_h + \frac{d}{T}\mu_\circ^4 H_{\rm eff}^3\Delta M + \frac{s}{T}\mu_\circ^4\alpha_h(\alpha_h + H_{\rm eff}\Delta M), \tag{48b}$$

and $\alpha_h = H_{\rm eff}(H_{\rm eff} + M_s)$, $T = t + d + s$, and $\tilde{\omega} = \omega/\gamma$. These equations are easily solved with the result

$$\omega_{1,2} = \gamma\left\{\frac{B \pm \sqrt{B^2 - 4C}}{2}\right\}^{1/2}. \tag{49}$$

The frequencies ω_1 and ω_2 represent the additional resonance frequency and the shifted FMR frequency. Using the same parameters used to obtain Fig. 7(b), we obtain similar FMR resonance frequencies as long as the ratio of thickness t, d, and s is the same as the ratio of the number of layers in the ferromagnet, the ferroelectric, and the normal metal.

Since the density of the screening charge can be increased by raising the external field, we expect that both the shift of the resonance frequency and the additional resonance frequency can be driven to higher values by increasing the external field. Using Fe as an electrode, we vary the external field E/E_b from 3.7% to 74%, and the frequency shift increases from 2 to 7.6 MHz. This is illustrated as a solid line in Fig. 9(a). Note that the weak additional frequency increases slightly from 28.80 to 28.92 MHz.

Next, we study the dependence of frequencies on the thickness of the ferroelectric. The electrode thickness and external field are set constant at 20 nm and $E/E_b = 44\%$. The ferroelectric thickness is increased by changing the number of layers from 100 to 700. This results in a decrease in the frequency shift from 5.7 to 1.8 MHz. This decrement also happens when the number of layers in the ferromagnet is increased. When we adjust the number of ferromagnet layers from 10 to 50 layers while holding the number of ferroelectric layers constant at 250, the shift of resonance frequency decreases from 11.3 to 2.8 MHz. This is consistent with the frequency shifts being due to the interface layer additional magnetization perturbation, which is significant only relative to the volume fraction of the additional layer magnetization and that of the remainder of the film.

As a final point, we compare the frequency shifts as a function of applied field of the FMR mode and the additional resonance for four different metallic ferromagnet electrodes in Figs. 9(a) and 9(b). The shift of FMR frequency has the largest value for CrO_2, and that for Fe has the smallest value. Since the FMR frequency is related to $H_a M_s$, it seems reasonable that the frequency shifts are related to $H_a \Delta M/M_s$, where $\Delta M/M_s$ represents the effect of the additional magnetization. Since the additional resonances are related to $H_a \Delta M$, then Fe has the largest additional resonance, and that for the Heusler alloy has the smallest value. In order to have a feeling for the magnitudes, we see that for $E/E_b = 15\%$, the largest additional magnetization is 3.7×10^4 A/m for CrO_2, and the smallest value is 8.7×10^3 A/m for Fe. The values at this field for the Heusler half metal and permalloy lie between these extremes, at 2.8×10^4 and 2.3×10^4 A/m.

V. CONCLUSIONS

We present a theory for magnetic resonance in ferromagnet/ferroelectric/normal metal trilayers biased by an applied voltage. We have shown how an additional magnetization is generated by the ferroelectric polarization at the ferromagnet interface, and that this can be measured indirectly through measurement of frequency shifts arising from a small induced moment on the ferromagnet. We predict the appearance of an additional weak resonance associated with the induced moment. We find that the frequency shifts depend on the magnitude of the additional magnetization and also the anisotropy field of the host. The shift of resonance frequency will be large if the fractional additional magnetization and host anisotropy fields are large. The possible application of these effects can be used in the signal processing where the frequency shift and the additional resonance frequency can be applied in the filtering process.

We have also explored the influence of additional magnetization on standing spin wave resonances. We find that the additional magnetization decreases pinning at the surfaces, which in turn distorts the mode profiles across the film thicknesses and increases the effective wavelength of the modes.

ACKNOWLEDGMENTS

We wish to acknowledge the support of Ausaid, the Australian Research Council, and DEST.

APPENDIX: ENERGY DENSITY FOR FERROELECTRICS WITH ELECTRODES

In this Appendix, we discuss the derivation proposed by Tilley[8] of the energy density of the system in which a ferroelectric is sandwiched between two metallic electrodes. The derivation in this appendix is based on Ref. 8. The calculation begins by treating the electric screening field in the Thomas-Fermi approximation:[9]

$$\frac{d^2E}{dx^2} = \frac{E}{\lambda^2}. \tag{A1}$$

Here λ represents the screening length of the electrode. For the case of two different electrodes, the boundary condition will be (using Mehta's configuration, as in Fig. 1)

$$E\left(\frac{\pm L}{2}\right) = 0 \quad \text{and} \quad E\left(\frac{\pm l}{2}\right) = \frac{\sigma_\pm}{\epsilon_\circ \epsilon_e^{r,l}}$$

with solution

$$E(x) = \frac{\sigma_\pm}{\epsilon_\circ \epsilon_e^{r,l} \sinh\left(\frac{L-l}{2\lambda_{r,l}}\right)} \sinh\left(\frac{\frac{1}{2}L \mp x}{\lambda_{r,l}}\right). \tag{A2}$$

The electrostatic energy inside the electrodes, determined by charge conservation $\sigma_+ = -\sigma_- = \sigma$, can be written as[8]

$$F_e = \frac{\epsilon_\circ}{2}\left\{\epsilon_e^l \int_{-L/2}^{-l/2} E_l^2 dx + \epsilon_e^r \int_{l/2}^{L/2} E_r^2 dx\right\} = \frac{\sigma^2}{2\epsilon_\circ}\gamma, \tag{A3}$$

where

$$\gamma = \left(\frac{\lambda_l}{\epsilon_l}\beta_l + \frac{\lambda_r}{\epsilon_r}\beta_r\right) \quad \text{and} \quad \beta_{l,r} = \frac{\sinh\left(\frac{L-l}{\lambda_{l,r}}\right) - \left(\frac{L-l}{\lambda_{l,r}}\right)}{\sinh^2\left(\frac{L-l}{2\lambda_{l,r}}\right)}. \tag{A4}$$

Next, we evaluate the electric field inside the ferroelectric. This is related to the polarization through the relation $\vec{\nabla}\cdot\vec{D}=0$, so

$$\epsilon_\circ\epsilon_f\frac{dE}{dx}=-\frac{dP}{dx}\quad\Rightarrow\quad E(x)=E_o-\frac{1}{\epsilon_\circ\epsilon_f}P(x). \tag{A5}$$

The electric field $E_\circ$ depends on the external potential $V_\circ$, which obeys the condition

$$\int_{-L/2}^{L/2}E(x)\,dx=-V_\circ. \tag{A6}$$

Substitution of the electric field in the electrodes and the ferroelectric in Eqs. (A2) and (A5) into the relation Eq. (A6), and also requiring continuity of D at $l/2$ and $-l/2$, results in

$$\epsilon_f E_\circ=\epsilon_e E_e\qquad\Rightarrow\qquad\sigma=\epsilon_\circ\epsilon_f E_\circ. \tag{A7}$$

Using this result in the expression for $E_\circ$ gives

$$E_\circ=\frac{1}{(\alpha+l)}\left\{\frac{1}{\epsilon_\circ\epsilon_f}\int_{-l/2}^{l/2}P dx-V_\circ\right\}, \tag{A8}$$

where

$$\alpha=\lambda_l\frac{\epsilon_f}{\epsilon_l}\frac{\cosh\left(\frac{L-l}{2\lambda_l}\right)-1}{\sinh\left(\frac{L-l}{2\lambda_l}\right)}+\lambda_r\frac{\epsilon_f}{\epsilon_r}\frac{\cosh\left(\frac{L-l}{2\lambda_r}\right)-1}{\sinh\left(\frac{L-l}{2\lambda_r}\right)}. \tag{A9}$$

By using Eq. (A8), the ferroelectric energy density in fourth order is[8]

$$F=\frac{1}{l}\int dx\left\{\frac{AP^2}{2}+\frac{BP^4}{4}+\frac{K}{2}\left(\frac{\partial P}{\partial x}\right)^2+\frac{P(x)}{2\epsilon_\circ\epsilon_f}\times\left[P(x)-\frac{l}{(\alpha+l)}\bar{P}\right]+\frac{V_\circ}{(\alpha+l)}P\right\}+\frac{K}{2\delta}(P_+^2+P_-^2). \tag{A10}$$

Then, the expression of the total energy density is obtained by adding the ferromagnet energy density in Eqs. (A3) and the ferroelectric energy density in Eq. (A10), yielding[8]

$$F=\int dx\left\{A\frac{P^2}{2}+B\frac{P^4}{4}+\frac{K}{2}\left(\frac{dP}{dx}\right)^2+\frac{2\pi}{\epsilon_f}P^2+\frac{V_\circ}{\alpha+l}P\right\}-\frac{2\pi}{\epsilon_f(\alpha+l)}\left[\int Pdx\right]^2+\frac{2\pi\gamma}{4(\alpha+l)^2}\left[\int Pdx\right]^2-\frac{\epsilon_f\gamma V_\circ}{4(\alpha+l)^2}\int Pdx+\frac{\epsilon_f^2\gamma}{4(\alpha+l)^2}\frac{V_\circ^2}{8\pi}+\frac{K}{2\delta}\left(P_+^2+P_-^2\right). \tag{A11}$$

This can be brought into the dimensionless form of Eq. (1) by defining the relation $P^2=P_\circ^2\tilde{P}^2$ with $P_\circ^2=\frac{a_\circ T_c}{B}$.

*slamev01@student.uwa.edu.au

[1] M. K. Niranjan, J. Burton, J. Velev, S. Jaswal, and E. Tsymbal, Appl. Phys. Lett. **95**, 052501 (2009).
[2] J. M. Rondinelli, M. Stengel, and N. A. Spaldin, Nat. Nanotech. **3**, 46 (2008).
[3] J. Lee, N. Sai, T. Cai, Q. Niu, and A. A. Demkov, Phys. Rev. B **81**, 144425 (2010).
[4] S. Zhang, Phys. Rev. Lett. **83**, 640 (1999).
[5] T. Cai, S. Ju, J. Lee, N. Sai, A. A. Demkov, Q. Niu, Z. Li, J. Shi, and E. Wang, Phys. Rev. B **80**, 140415 (2009).
[6] M. Y. Zhuravlev, S. Maekawa, and E. Y. Tsymbal, Phys. Rev. B **81**, 104419 (2010).
[7] R. Mehta, B. Silverman, and J. Jacobs, J. Appl. Phys. **44**, 3379 (1973).
[8] D. R. Tilley, in *Phase Transition in Thin Film*, edited by N. Setter and E. Colla (Birkhauser Verlag, Basel, 1993), pp. 163–83.
[9] C. Kittel, *Introduction to Solid State Physics*, 6th ed. (Wiley, New York, 1986), p. 264.
[10] B. Kuanr, I. R. Harward, D. L. Marvin, T. Fal, R. E. Camley, D. L. Mills, and Z. Celinski, IEEE Trans. Magn. **41**, 3538 (2005).
[11] G. Liu and C.-W. Nan, J. Phys. D **38**, 584 (2005).
[12] R. Kretschmer and K. Binder, Phys. Rev. B **20**, 1065 (1979).
[13] J. M. D. Coey and M. Venkatesan, J. Appl. Phys. **91**, 8345 (2002).
[14] J. M. D. Coey, A. E. Berkowitz, L. I. Balcells, F. F. Putris, and A. Barry, Phys. Rev. Lett. **80**, 3815 (1998).
[15] R. Cheng, Z. Liu, X. Bo, S. Adenwalla, L. Yuan, S. Liou, and P. Dowben, Mater. Lett. **56**, 295 (2002).
[16] X. Zou and G. Xiao, Appl. Phys. Lett. **91**, 113512 (2007).
[17] S. Picozzi, A. Continenza, and A. Freeman, J. Phys. D **40**, 851 (2006).
[18] D. Sprungmann, K. Westerholt, and H. Zabel, Superlattices Microstruct. **41**, 146 (2007).
[19] P. Webster, J. Phys. Chem. Solids **32**, 1221 (1971).
[20] M. Belmeguenai, F. Zighem, G. Woltersdorf, Y. Roussigne, S. Cherif, K. Westerholt, and G. Bayreuther, J. Magn. Magn. Mater. **321**, 750 (2009).
[21] S. Ostanin, J. Staunton, S. Razee, B. Ginatempo, and E. Brunol, J. Magn. Magn. Mater. **295**, 110 (2005).
[22] R. Magaraggia, K. Kennewell, M. Kostylev, R. L. Stamps, M. Ali, D. Greig, B. J. Hickey, and C. H. Marrows, Phys. Rev. B **83**, 054405 (2011).
[23] C.-G. Duan, C.-W. Nan, S. S. Jaswal, and E. Y. Tsymbal, Phys. Rev. B **79**, 140403 (2009).
[24] N. S. Almeida and D. L. Mills, Phys. Rev. B **37**, 3400 (1988).
[25] N. Raj and D. R. Tilley, Phys. Rev. B **36**, 7003 (1987).
[26] R. L. Stamps, R. E. Camley, F. C. Nortemann, and D. R. Tilley, Phys. Rev. B **48**, 15740 (1993).
[27] R. L. Stamps and R. E. Camley, Phys. Rev. B **54**, 15200 (1996).
[28] K. L. Livesey and R. L. Stamps, Phys. Rev. B **81**, 094405 (2010).
[29] G. T. Rado and J. R. Weertman, J. Phys. Chem. Solids **11**, 315 (1959).